Critical dynamics at the Anderson localization mobility edge

Cord A. Müller,[1] Dominique Delande,[2] and Boris Shapiro[3]

[1]*Fachbereich Physik, Universität Konstanz, 78457 Konstanz, Germany*

[2]*Laboratoire Kastler Brossel, UPMC-Sorbonne Universités, CNRS, ENS-PSL Research University,*
Collège de France, 4 Place Jussieu, 75005 Paris, France

[3]*Department of Physics, Technion–Israel Institute of Technology, Haifa 32000, Israel*

We study the critical dynamics of matter waves at the three-dimensional Anderson mobility edge in cold-atom disorder quench experiments. General scaling arguments are supported by precision numerics for the spectral function, diffusion coefficient, and localization length in isotropic blue-detuned speckle potentials. We discuss signatures of critical slowdown in the time-dependent central column density of a spreading wave packet, and evaluate the prospects of observing anomalous diffusion right at criticality.

I. INTRODUCTION

Anderson localization refers to the remarkable phenomenon that configurational disorder can keep a phase-coherent system out of global equilibrium, with the eventual consequence that diffusive transport is entirely suppressed and thus resulting in an insulator [1,2]. Quantum systems show in dimensions $d > 2$ an Anderson transition [3,4], a critical change of transport properties from insulating to conducting that is rooted in the existence of a mobility edge E_c, a critical point on the single-particle energy axis that separates localized from extended states. Since disordered electrons invariably interact [5,6], making the unambiguous observation of the single-particle scenario very difficult, other physical carriers with much weaker interaction have been used to track the three-dimensional (3D) Anderson transition: acoustic waves [7], light waves [8,9] (but see [10]), and cold atoms [11–13]. Notably, the universality and critical properties of the 3D Anderson transition have been thoroughly investigated with the quantum kicked rotor, a driven chaotic system, where localization operates in momentum space [14,15]. Also cold-atom real-space experiments [16–18] have attempted to measure the mobility edge in spatially correlated laser speckle potentials. The basic idea of these wave-packet expansion experiments is that mobile atoms with energies $E > E_c$ above the mobility edge escape, whereas localized atoms with energies $E < E_c$ remain behind. From the measured localized fraction and initial energy distribution, one can then deduce the mobility edge.

Concretely, let us assume that matter waves are prepared at time $t = 0$ with an uncorrelated phase-space density $W(\mathbf{k},\mathbf{r}) = w(\mathbf{k})n_0(\mathbf{r})$ [17,19] and resulting energy distribution $A(E) = \int d\mathbf{k} A(\mathbf{k},E)w(\mathbf{k})$; the conditional probability $A(\mathbf{k},E)$ of a plane wave $\mathbf{k}$ to have energy E in the disorder potential is the spectral function. The ensemble-averaged atom density at position $\mathbf{r}$ and time $t > 0$ is

$$n(\mathbf{r},t) = \int dE\, A(E) \int d\mathbf{r}_0\, P(E,\mathbf{r} - \mathbf{r}_0,t)n_0(\mathbf{r}_0), \quad (1)$$

where $P(E,\mathbf{r} - \mathbf{r}_0,t)$ is the density (particle-hole) quantum propagator at energy E from $\mathbf{r}_0$ to $\mathbf{r}$ in time t [4,20,21]. The fraction of localized atoms, among all $N = \int d\mathbf{r}_0 n(\mathbf{r}_0)$ atoms

initially present, then formally evaluates to

$$f_{\text{loc}} = \frac{1}{N} \int d\mathbf{r} \lim_{t \to \infty} n(\mathbf{r},t) = \int_{-\infty}^{E_c} dE\, A(E), \quad (2)$$

where the last equality uses the long-time projection $\int d\mathbf{r} \lim_{t \to \infty} P(E,\mathbf{r},t) = \Theta(E_c - E)$ onto energies below the mobility edge. If the energy distribution $A(E)$ is known and covers the mobility edge, one can infer the position of E_c from the measured value f_{loc}.

In an actual experiment, it is crucial to know how long one has to wait for Eq. (2) to be valid, i.e., until the density of mobile atoms has dropped to zero in a given observation volume. Likewise, one has to ascertain carefully whether density profiles observed at finite times represent localized states, or rather comprise atoms that still diffuse, if only very slowly [22–25]. Strictly speaking, the disappearance of the mobile fraction takes an infinite time since the diffusion coefficient becomes critically small near E_c. A density measurement at a finite observation time then runs the danger of counting a certain, potentially sizable, fraction of mobile atoms as localized, resulting via Eq. (2) in an estimate for the mobility edge that is systematically too high. This effect may be one of the reasons why the experimental estimates for localized fractions and mobility edges of Refs. [16–18] are consistently above recent, accurate numerical estimates [26]. Even if there existed a general awareness that critical dynamics come with diverging time and length scales, appropriate quantitative conclusions seem not to have been drawn. Finally, similar considerations should apply to the experimental characterization of the many-body localization transition [27–31], where subdiffusive transport is also expected to occur [32–37].

With this article, we wish to emphasize the principal as well as practical relevance of critical dynamics around the 3D Anderson mobility edge in disorder-quench, matter-wave expansion experiments. This analysis significantly extends previous theories [21,22,38–40] that used various versions of the self-consistent theory of localization, with largely uncontrolled approximations regarding the spectral function, critical exponents, and position of the mobility edge. Indeed, in Sec. II we illustrate our general arguments with precise numerical results for the spectral function, average density of states, diffusion coefficient, and localization length in 3D

blue-detuned speckle disorder, as appropriate for present-day experiments. We do not attempt a quantitative comparison to one of the existing experiments [16–18] since each of them uses its own particular preparation, measurement protocol, and disorder configuration. Rather, our analysis relies on generic assumptions that represent the smallest common denominator for the existing cases, and it may thus serve as a conceptual guide rail for a more accurate analysis of experiments yet to come. Section III discusses the relevant time and length scales for the critical dynamics of a spreading wave packet. We focus our discussion on the central column density, arguably a more trustworthy observable than small wing densities, and finally evaluate the prospects of observing anomalous diffusion right at criticality. Section IV concludes.

II. CRITICAL ENERGY AND TIME SCALES

A. Anderson localization in 3D speckle disorder

Let $V(\mathbf{r})$ denote a realization of a random, blue-detuned optical speckle potential [12,21]. We assume that the disorder is statistically isotropic and homogeneous, leaving aside aspects such as anisotropy and finite size that may be relevant to particular experimental configurations. The mean $\overline{V(\mathbf{r})}$ or "sea level" can be put to 0 without loss of generality, counting energies now from this level. The disorder strength is then defined by the variance $\overline{V(\mathbf{r})^2} = V_0^2$. Higher-order moments of the single-point potential values $V = V(\mathbf{r})$ are fully characterized by the statistical distribution function $P(V)$. The blue-speckle distribution is strictly bounded from below and has the negative-exponential distribution $P(V) = \Theta(V + V_0)V_0^{-1} \exp[-(V + V_0)/V_0]$.

Spatial correlations are captured by the covariance $\overline{V(\mathbf{r})V(\mathbf{r}')} = V_0^2 C(\mathbf{r} - \mathbf{r}')$. For concreteness, we consider the Gaussian correlation $C(\mathbf{r}) = \exp[-\mathbf{r}^2/2\zeta^2]$. Such a correlation is *generic*, defined by the property $\int d\mathbf{r} C(\mathbf{r}) = \widetilde{C}(\mathbf{k} = 0) < \infty$, such that a white-noise description is applicable in the limit $k\zeta \ll 1$. Experimentally, Gaussian correlation is relevant in the plane perpendicular to a focused laser beam with Gaussian intensity waist, and approximately isotropic 3D speckle potentials are created superposing several such patterns [17,18] [41]. The correlation length defines the quantum correlation energy scale $E_\zeta = \hbar^2/m\zeta^2$.

In the (semi-)classical limit $V_0 \gg E_\zeta$ localization occurs very close to the classical percolation threshold where $k\zeta \gg 1$, such that quantum interference effects are very small [12]. We believe that expansion experiments in this regime [16,23] have mainly probed diffusive dynamics [24,25]. Here, we consider the opposite regime

$$\eta = \frac{V_0}{E_\zeta} \ll 1. \tag{3}$$

As a consequence, the potential cannot produce locally bound states, and localization of matter waves becomes a quantum-mechanical, multiple-scattering effect, known as *Anderson localization* (AL).

It is by now established that the mobility edge E_c for blue-detuned speckle is located slightly below the sea level $\overline{V} = 0$. This has been predicted by approximate but sufficiently accurate treatments like the self-consistent theory of

localization [39,42] [43] and confirmed by exact numerical calculations [26]. It also follows by a qualitative reasoning from the celebrated Ioffe-Regel criterion, which states that the Boltzmann description of classical transport has to be abandoned, and quantum effects may be expected to take over, once the wavelength becomes of the order of the mean-free path, $k_c l_c \sim 1$. For the generic class of disorder and high energies well above sea level, the perturbation-theory mean-free path $l \sim \zeta/\eta^2$ is independent of energy. Extrapolated to $l \sim l_c$, the Ioffe-Regel criterion then yields a characteristic energy scale $\hbar^2 k_c^2/2m \sim W$ such that [44]

$$W \sim \eta^4 E_\zeta = \eta^3 V_0. \tag{4}$$

The mobility edge E_c itself then can be expected to lie near the energy that solves the disorder-shifted dispersion relation for this momentum $k_c \sim l_c^{-1}$. Since the disorder shifts the bulk dispersion downward by the real part of the self-energy, $\Delta E \sim -\eta^2 E_\zeta$, which is larger in magnitude than W for $\eta \ll 1$, the mobility edge finally ends up below sea level. We recall that the same scale W is identified by a Lifshitz-tail argument coming from low energies [12]. It is thus plausible to assume that W is the single characteristic energy scale around E_c, where quantum interference effects play a crucial role, and thus yields an order of magnitude for the width of the critical interval. Although W is rather small on both scales of E_ζ and V_0 in the regime of interest $\eta \ll 1$, it can have a considerable impact on matter wave expansion dynamics, as shown in the following.

B. Critical interval

We proceed by presenting numerical data that prove the relevance of the critical interval around the 3D mobility edge. Our calculations use the single-particle Hamiltonian $H = \mathbf{p}^2/2m + V(\mathbf{r})$ of matter waves in blue-detuned speckle disorder with $\eta = V_0/E_\zeta = 0.5$. Figure 1 shows the spectral function $A(0, E)$ at zero momentum. The numerical routine propagates the initial state $|\mathbf{k} = 0\rangle$ in time with the Hamiltonian H for each realization, followed by a Fourier transformation to energy and an ensemble average. The system size is chosen much larger than the scattering mean free path, the spatial discretization much smaller than the correlation length ζ, and the results are averaged over many disorder realizations, so that all results shown in Fig. 1 have error bars smaller than 1% of their maximal value; further details can be found in the appendix of Ref. [45].

The spectral function thus obtained approximates the energy distribution $A(E)$ relevant for Eqs. (1) and (2) if the initial momentum distribution $w(\mathbf{k})$ is centered on $\mathbf{k} = 0$ and narrow enough. Indeed, the width of the spectral function $A(k, E)$ around $E = E_c$ is of the order of $l_c^{-1} \sim \eta^2/\zeta$. If the width Δk_0 of the initial distribution $w(\mathbf{k}_0)$ obeys $\Delta k_0 l_c \ll 1$, then $A(E) = \int d\mathbf{k} w(\mathbf{k})A(\mathbf{k}, E) \approx A(0, E)$. Initial momentum distributions that are centered on finite $|\mathbf{k}_0| > l_c^{-1}$ or that are much broader would provide a less optimal coverage of the mobility edge and will not be considered in the following.

The upper inset of Fig. 1 shows the average density of states per volume $\rho(E)$, which starts with an exponentially small Lifshitz tail [12,46,47] from the exact lower bound of the spectrum at $-V_0 = -0.5E_\zeta$ (the combined lower bound of
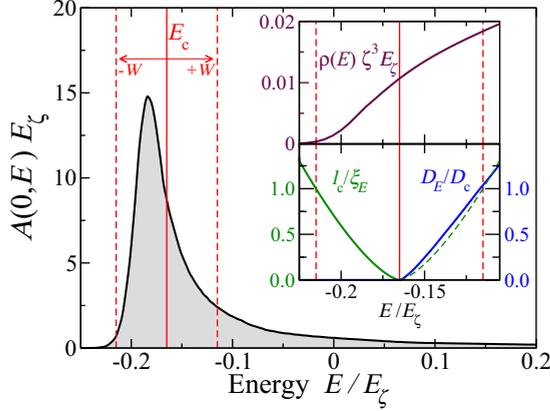
FIG. 1. Main plot: Spectral function $A(0,E)$ of a matter wave with $\mathbf{k}=0$ inside a blue-detuned laser speckle potential of zero mean and rms strength $V_0 = 0.5 E_\zeta$; the unit of energy $E_\zeta = \hbar^2/m\zeta^2$ is set by a generic spatial Gaussian correlation length ζ. The 3D Anderson mobility edge at $E_c \approx -0.1652 E_\zeta$ (red vertical line) lies below the "sea level" or potential mean at $E = 0$. The critical interval with half width $W = 0.05 E_\zeta$ (dashed vertical lines) contains initially more than two thirds of atoms; less than half of all atoms, with energy $E < E_c$, will eventually be localized. Insets: Zoom in the critical interval with plots of the smooth average density of states $\rho(E)$, critical inverse localization length ξ_E^{-1}, and critical diffusion coefficient D_E, in units of l_c and $D_c = \hbar/3m$.

kinetic energy and centered blue-speckle potential) and crosses over to the high-energy asymptotics $\propto E^{1/2}$ of the Galilean dispersion $E(\mathbf{p}) = \mathbf{p}^2/2m$ in 3D. An extrapolation of this bulk density of states to 0 gives an apparent lower band edge near $\Delta E \approx -0.20 E_\zeta$.

The spectral function and the average density of states are smooth functions of energy around the mobility edge E_c that separates localized states with $E < E_c$ from extended states with $E > E_c$ [26,48]. But transport coefficients show critical power-law behavior on both sides of E_c, found here at $E_c \approx -0.1652 E_\zeta$, as shown in the lower inset of Fig. 1. The half width of the critical interval appears to be $W \approx 0.05 E_\zeta$, in agreement with the estimate (4). As the energy approaches the mobility edge E_c from below, the localization length diverges like

$$\xi_E \sim l_c \left(\frac{W}{E_c - E}\right)^\nu, \quad -W < E - E_c < 0, \quad (5)$$

with critical exponent $\nu \approx 1.58$ known only from numerical and laboratory experiments [15,49–52]. The length l_c is of the order of the elastic scattering length, a smooth function of energy at the transition. For our parameters, we find $l_c \approx 4\zeta$, which complies with the Ioffe-Regel criterion $k_c l_c \sim 1$, with $\hbar k_c = \sqrt{2mW}$ the typical momentum at E_c.

As the energy approaches E_c from above, the diffusion coefficient vanishes as

$$D_E \sim D_c \left(\frac{E - E_c}{W}\right)^s, \quad 0 < E - E_c < W. \quad (6)$$

The critical exponents in Eqs. (5) and (6) are related by Wegner's law [53] $s = (d-2)\nu$, and thus $s = \nu$ in the present context. The diffusion coefficient reaches the "quantum unit

of diffusion" $D_c = \hbar/3m$ around the energy $E_c + W$ above the transition. We write $D_c = l_c^2/\tau_c$ with τ_c of the order of the elastic scattering time, also a smooth function of energy around E_c.

Numerically, we compute the critical quantities by a transfer-matrix calculation of the quasi-1D localization length $\xi_E(M)$ in a slab of transverse size M, extrapolated by finite-size scaling to the large-M limit [54,55]. Below E_c, the 3D bulk localization length $\xi_E = \lim_{M \to \infty} \xi_E(M)$ is finite. Above E_c, it is the localization length per cross section, $\xi_E'^{-1} = \lim_{M \to \infty} \xi_E(M)/M^2$, that is finite and plotted as the green dashed curve in the lower inset of Fig. 1. This length scale then gives the bulk diffusion coefficient as $D_E = [\pi \hbar \rho(E) \xi_E']^{-1}$ [56]. One-parameter scaling actually constrains the critical exponents of ξ_E and ξ_E' to be equal, but since in our case $\rho(E)$ is not strictly constant over the full critical interval, D_E does not obey the simple power law (6) everywhere with the same $s = \nu$. Rather, Fig. 1 displays a crossover for D_E from a linear behavior with $s \approx 1$ at higher energies toward the true $s = \nu$ close enough to E_c, which is relevant for the long-time dynamics.

For our showcase data of Fig. 1, the initial energy distribution $A(E)$ is composed of the regular localized fraction $f_{\text{loc}}^{\text{reg}} = A_{-\infty}^{E_c-W} \approx 0.004$ [we note $A_a^b = \int_a^b dE\, A(E)$], a critical localized fraction $f_{\text{loc}}^{\text{crit}} = A_{E_c-W}^{E_c} \approx 0.453$, a critical diffusive fraction $f_{\text{diff}}^{\text{crit}} = A_{E_c}^{E_c+W} \approx 0.233$, and a regular diffusive fraction $f_{\text{diff}}^{\text{reg}} = A_{E_c+W}^{\infty} \approx 0.310$. Clearly, for disorder strengths and energy distributions comparable to the above, we may expect the critical region to play an important role since it contains a total critical fraction of $f^{\text{crit}} = f_{\text{loc}}^{\text{crit}} + f_{\text{diff}}^{\text{crit}} \approx 0.686$, i.e., more than two thirds of all atoms.

C. Anomalous dynamics at finite times

As the wave packet expands, the dynamics progressively distinguishes between the total localized fraction $f_{\text{loc}} = f_{\text{loc}}^{\text{reg}} + f_{\text{loc}}^{\text{crit}} \approx 0.457$ and the total diffusive fraction $f_{\text{diff}} = f_{\text{diff}}^{\text{reg}} + f_{\text{diff}}^{\text{crit}} \approx 0.543$. Yet, in any experiment that probes dynamics of a wave packet during a finite time t, it is impossible to sharply distinguish between localized and diffuse contributions near E_c, since the resolution in energy is necessarily limited. Instead, energy components near criticality show a crossover behavior of anomalous diffusion [57,58], characterized by the subdiffusive law $\langle |x| \rangle \sim l_c (t/\tau_c)^{1/3}$ that interpolates between the truly diffusive and strongly localized regimes, where $\langle |x| \rangle \sim l(t/\tau)^{1/2}$ and $\langle |x| \rangle \sim \xi t^0$, respectively.

One can estimate the half width $\delta E(t)$ of the anomalous energy interval by requiring that the critical localization length at energy $E_c - \delta E$ is reached at time t by anomalous diffusion, $\xi_{E_c-\delta E} = l_c (t/\tau_c)^{1/3}$. Solving for δE with Eq. (5), one finds

$$\frac{\delta E(t)}{W} = \left(\frac{\tau_c}{t}\right)^{\frac{1}{3\nu}} =: \Delta(t). \quad (7)$$

Alternatively, this scale emerges by requiring that localization and diffusion cannot be distinguished, i.e., by equating $\xi_{E_c-\delta E}$ with the critical diffusive radius at energy $E_c + \delta E$ and time t. Solving $D_{E_c+\delta E} t = \xi_{E_c-\delta E}^2$ for δE with the help of Eqs. (5) and (6) then yields Eq. (7) as well.
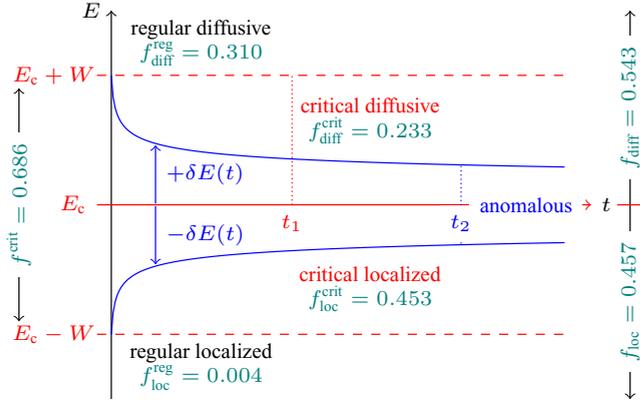
FIG. 2. Energy interval around the mobility edge E_c and different dynamical regimes. Numerical figures for the respective fractions are indicated for the showcase data of Fig. 1. The half width of the anomalous interval shrinks as $\delta E(t) = W(\tau_c/t)^{1/3\nu}$, Eq. (7). A spatial cutoff scale σ_0 (width of the initial wave packet if the central column density is monitored) introduces two crossover times: (1) The upper critical Thouless time $t_1 = \sigma_0^2/D_c$, Eq. (8), separates regular from critical diffusion. (2) The localization time $t_2 = t_1\sigma_0/l_c$, Eq. (9), separates critical from anomalous dynamics.

The anomalous energy interval shrinks as a function of time, as shown schematically in Fig. 2, so that more and more particles are resolved as either localized or diffusive. But the anomalous energy interval shrinks very slowly, and only at infinitely long times does the separation between localized and mobile components become infinitely sharp.

D. Finite spatial resolution and crossover times

In real-life expansion experiments, the dynamics are limited not only temporally, but also spatially. For example, measurements of the total remaining numbers of particles [16,18] can only cover a finite observation range. Similarly, measurements of central densities [17] start from clouds with finite initial extension. Let us call σ_0 the corresponding spatial scale, and assume $\sigma_0 \gg l_c$, which proves compatible with the assumption $\Delta k_0 l_c \ll 1$ made for the momentum distribution in Sec. II B above. The length σ_0 then introduces two characteristic crossover times that separate three different dynamical regimes, as schematically indicated in Fig. 2.

First, there is the upper critical Thouless time

$$t_1 = \frac{\sigma_0^2}{D_c} = \tau_c \frac{\sigma_0^2}{l_c^2}, \tag{8}$$

namely, the time required for the fastest critical, or slowest regular, diffusive atoms with diffusion coefficient D_c to explore the scale σ_0. Starting with a broad enough energy distribution, the early-time dynamics will be dominated by rapid, regular diffusion for $t \ll t_1$, and cross over to slower, critical diffusion for $t \gg t_1$. As an order of magnitude, a value as large as 40 s can be realistic, taking the Palaiseau experiment [17] as reference where $D_c \approx 0.25~\mu\mathrm{m}^2/\mathrm{ms}$ and $\sigma_0 \approx 100~\mu\mathrm{m}$ is the initial wave-packet size.

Second, there is the time t_2 required for the slowest critical, or fastest anomalous, atoms with energy $E_c + \delta E(t_2)$ to reach σ_0. Using Eqs. (6) and (7), this translates to the condition

$\sigma_0^2 = t_2 D_c \Delta(t_2)^\nu$. Equivalently, t_2 is the time where the localization length at $E_c - \delta E(t_2)$ reaches σ_0. Both conditions agree on the "localization time" [22]

$$t_2 = \tau_c \frac{\sigma_0^3}{l_c^3} = t_1 \frac{\sigma_0}{l_c}, \tag{9}$$

or "watershed time" when the difference between localized and mobile components on the spatial scale σ_0 is resolved. From t_2 onward, the localized components with $\xi_E < \sigma_0$ are essentially frozen, the diffusive components with $D_E > \sigma_0^2/t$ have essentially left, and the only remaining dynamics is due to the anomalous diffusion of a small fraction of particles with even larger critical localization lengths and smaller critically diffusive radii.

In summary, one expects a double dynamical crossover [22]: first from fast, regular diffusion at times $t \ll t_1$ to slow, critical diffusion at times $t_1 \ll t \ll t_2$ and then to anomalous behavior for very long times $t \gg t_2$.

III. CENTRAL COLUMN DENSITY

As a consequence of the previous considerations and associated long time scales, it becomes plausible that experiments tend to overestimate the localized fraction and thus yield values for E_c that are systematically too high. Clearly, one needs to extrapolate finite-time, finite-size data quite carefully in order to arrive at accurate estimates of the localized fraction. To facilitate this, we follow the general lines of Skipetrov et al. [22], but instead of analyzing the sparse tails of expanding density distributions, we propose to monitor the decrease of the central column density at $x = y = 0$,

$$n^\perp(t) := \int dz\, n(0,0,z,t), \tag{10}$$

from its initial value $n_0^\perp = n^\perp(0)$ as function of time. The central column density, with its higher signal-to-noise ratio than the wing density, has been used with success in dynamical localization experiments [14,58], and promises to be useful in real space as well [17].

Whereas the localized component $n_{\mathrm{loc}}^\perp = f_{\mathrm{loc}} n_0^\perp$ remains essentially immobile from the start (to good approximation if $l_c \ll \sigma_0$ and thus $\xi_E \lesssim \sigma_0$ for the majority of localized atoms), the mobile component will escape, and thus its contribution to the central column density will decrease in time.

We consider a wave packet prepared in a system so large that ballistic modes are not populated. Let us also, in a first step, be deliberately oblivious of the anomalous dynamics and assume diffusion above E_c at all times by taking $\delta E(t) = 0$; the signatures of anomalous dynamics will be discussed in Sec. III B below. In the diffusive interval $E > E_c$, the density propagator then is the Gaussian diffusion kernel

$$P(E,\mathbf{r},t) = (4\pi D_E t)^{-\frac{3}{2}} \exp(-\mathbf{r}^2/4D_E t). \tag{11}$$

Assuming an initial isotropic Gaussian distribution

$$n_0(\mathbf{r}) = \frac{N}{(2\pi\sigma_0^2)^{3/2}} \exp\left(-\mathbf{r}^2/2\sigma_0^2\right), \tag{12}$$

for which $n_0^\perp = N/2\pi\sigma_0^2$, one finds from Eqs. (1) and (10) by Gaussian integration

$$n^\perp(t) = n_{\text{loc}}^\perp + N \int_{E_c}^\infty \frac{dE}{2\pi} \frac{A(E)}{\sigma_0^2 + 2D_E t}. \qquad (13)$$

If there were a finite time scale $t^* = \max_E \sigma_0^2/D_E$ for all energies contained in the distribution $A(E)$ above E_c, one would find for $t \gg t^*$ an asymptotic algebraic decrease like

$$n^\perp(t) \approx f_{\text{loc}} n_0^\perp + \frac{N\langle D_E^{-1}\rangle}{4\pi t} + O(t^{-2}), \qquad (14)$$

where $\langle D_E^{-1}\rangle = \int_{E_c}^\infty dE A(E) D_E^{-1}$. A $1/t$ power-law fit could then reveal the constant offset and thus permit one to extract f_{loc}, as in Ref. [17]. However, this approach neglects the critical behavior at the mobility edge. Indeed, whenever $A(E)$ is finite around E_c, the average of the inverse critical diffusion coefficient is ill defined since

$$\langle D_E^{-1}\rangle \propto \int_{E_c} \frac{dE\, A(E)}{(E - E_c)^\nu} \sim (E - E_c)^{1-\nu}|_{E_c} \to \infty. \qquad (15)$$

It is actually impossible to enter the supposed long-time regime $t \gg t^*$ because $\sigma_0^2/D_E \to \infty$ as $E \to E_c$, and the time required for the escape of all mobile atoms diverges as their energy approaches E_c from above.

Of course, the argument leading to Eq. (14) can be applied to the contribution of the *regular diffusive* atoms with energies $E > E_c + W$ and diffusion coefficients $D_E > D_c$. For these atoms, $t^* = \sigma_0^2/D_c = t_1$ is the upper critical Thouless time defined in Eq. (8), and thus their contribution to Eq. (13) vanishes like t_1/t for $t \gg t_1$.

The regular diffusive atoms thus give way to the critically diffusive atoms with energies $E_c < E < E_c + W$ that take longer to disappear. In the following, we discuss more quantitatively the contribution of critical dynamics to the central column density, dominant at times $t \gg t_1$, all the way to the anomalous diffusion at criticality that dominates at even longer times $t \gg t_2$.

A. Critical diffusion

For the qualitative analysis of the expected critical dynamics, let us take the energy distribution $A(E) \approx A(E_c) =: A_c$ to be constant in the narrow critical interval above E_c. There, the diffusion coefficient is $D_E = D_c\Delta^\nu$, where $\Delta = (E - E_c)/W \in [0,1]$ measures the distance to the critical point. The critically diffusive atoms with energies $E \in [E_c, E_c + W]$ then contribute to the central column density [Eq. (13)] with

$$n_{\text{diff}}^\perp(t) \approx n_0^\perp W A_c \int_0^1 \frac{d\Delta}{1 + 2(t/t_1)\Delta^\nu}. \qquad (16)$$

We only need to estimate the integral for times $t \gg t_1 = \sigma_0^2/D_c$, when the regularly diffusive atoms have already disappeared. The integral is dominated by the behavior of the integrand near the lower bound and results in the algebraic decay

$$n_{\text{diff}}^\perp(t) \sim n_0^\perp \left(\frac{t_1}{t}\right)^{\frac{1}{\nu}}, \quad t_1 \ll t \ll t_2, \qquad (17)$$
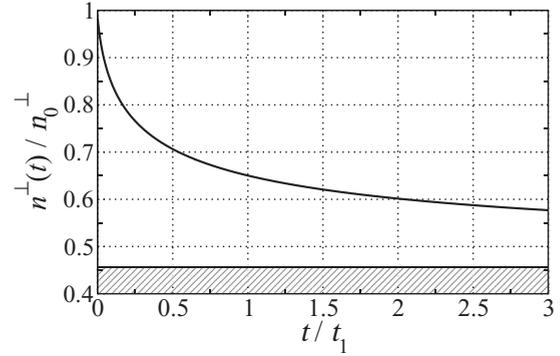
FIG. 3. Central column density, Eq. (13), evaluated for the data of Fig. 1, as function of time. Around the upper critical Thouless time $t_1 = \sigma_0^2/D_c$, the fraction of regular diffusive atoms (here $f_{\text{diff}}^{\text{reg}} \approx 0.31$) has almost disappeared, and the slow critical diffusion of Eq. (17) starts to dominate. Anomalous diffusion becomes only relevant at much longer times $t \gg t_2 = \sigma_0 t_1/l_c$. Especially with noise on the data, one could be tempted to extrapolate the curve to a localized fraction of 0.52 or more; in reality, it is only $f_{\text{loc}} = 0.457$, indicated by the shaded baseline.

where constants of order unity, WA_c among them, are omitted. This power-law decay involving the critical exponent ν is much slower than the faster t^{-1} decay of the regular diffusion, and consequently is quite easily mistaken for a saturation due to Anderson localization.

To underscore this point, Fig. 3 plots the central column density, Eq. (13), as function of time for the parameters of Fig. 1. Around t_1, the fraction of regular diffusive atoms (here $f_{\text{diff}}^{\text{reg}} \approx 0.31$) has almost disappeared, and slow critical diffusion starts to dominate. It must be noted that the argument leading to the power-law prediction (17) slightly oversimplifies the actual situation. Since the spectral function $A(0,E)$ varies notably over the upper critical interval (see Fig. 1), the approximation (16) is not very accurate at early times of order t_1. Also, the caveat of [41] applies such that the pure power law of Eq. (17) is only reached rather slowly. Still, even if Fig. 3 does not admit a global fit to the simple analytical estimate of Eq. (17), the overall critical slowdown is clearly visible. Especially if the data were noisy for longer times, a naive fit to a t^{-1} power law would yield a measured localized fraction of 0.52 or more, significantly larger than its true value $f_{\text{loc}} = 0.457$.

How long does this critical decay last? Until here, we have neglected anomalous diffusion. Reinserting the true lower bound of the critical diffusion interval at $E_c + W\Delta(t)$, the integral to be evaluated in Eq. (16) is really only

$$\int_{\Delta(t)}^1 \frac{d\Delta}{1 + 2(t/t_1)\Delta^\nu}. \qquad (18)$$

The value of the integral for $t \gg t_1$ depends on the larger of the two cutoffs, either 1 or $(t/t_1)\Delta(t)^\nu$. A crossover time t_2 between these two cases is defined by the condition $\Delta(t_2)^\nu = t_1/t_2$, which yields Eq. (9). At intermediate times $t_1 \ll t \ll t_2$ such that t_1/t is always greater than $\Delta(t)^\nu$, the lower integral bound can be set to zero; here the contribution of anomalous atoms is negligible, and the dynamics is indeed dominated by the critical diffusion of Eq. (17).

At even longer times $t \gg t_2$, the integral in Eq. (16) is exhausted by values close to its lower bound where $(t/t_1)\Delta(t)^\nu \gg 1$. With its upper bound sent to infinity, the integral then evaluates to $\Delta(t)^{1-\nu}/(\nu - 1)$, and one obtains the long-time algebraic behavior

$$n_{\text{diff}}^\perp(t) \sim n_0^\perp \Delta(t_2)\left(\frac{t_2}{t}\right)^{\frac{1+2\nu}{3\nu}}, \quad t_2 \ll t. \quad (19)$$

Actually, this is the regime where anomalous diffusion becomes relevant, to be discussed next.

B. Anomalous diffusion

Allowing for a frequency-dependent diffusion coefficient $D_E(\omega)$ in the Fourier-transformed diffusion kernel $P(E,\mathbf{q},\omega) \propto [D_E(\omega)\mathbf{q}^2 - i\omega]^{-1}$ [20], one can write the diffusion propagator

$$P(E,\mathbf{r},t) = \int \frac{d\omega}{2\pi} \frac{\exp\{-i\omega t - |\mathbf{r}|\sqrt{-i\omega/D_E(\omega)}\}}{4\pi D_E(\omega)|\mathbf{r}|}. \quad (20)$$

Scaling theory and microscopic calculations [59] have established that the frequency-dependent diffusion coefficient $D_E(\omega)$ at the mobility edge is

$$D_{E_c}(\omega) = D_c(-i\omega\tau_c)^{1/3}, \quad (21)$$

whence Eq. (20) turns into the critical diffusion propagator

$$P_c(\mathbf{r},t) = \frac{1}{4\pi D_c|\mathbf{r}|} \int \frac{d\omega}{2\pi} \frac{\exp\{-i\omega t - (-i\omega\tau_c)^{1/3}|\mathbf{r}|/l_c\}}{(-i\omega\tau_c)^{1/3}}. \quad (22)$$

This expression, formally independent of energy, holds in the range $\pm\delta E(t) = \pm W\Delta(t)$ around the mobility edge. Its contribution to the central column density then is

$$n_c^\perp(t) = 2WA_c\Delta(t)\int dz \int d\mathbf{r}_0 n_0(\mathbf{r}_0)P_c(|\hat{\mathbf{z}} - \mathbf{r}_0|,t), \quad (23)$$

where $\hat{\mathbf{z}} = (0,0,z)$. Using translation invariance $\int d\mathbf{r}_0 n_0(\mathbf{r}_0)P(|\mathbf{r} - \mathbf{r}_0|) = \int d\mathbf{r}_0 n_0(\mathbf{r}_0 + \mathbf{r})P(|\mathbf{r}_0|)$ and the initial distribution (12), we can perform the Gaussian integral over z and thus face the task to evaluate

$$n_c^\perp(t) = 2n_0^\perp WA_c\Delta(t)\int d\mathbf{r}_0 \exp\left\{-\frac{x_0^2 + y_0^2}{2\sigma_0^2}\right\}P_c(|\mathbf{r}_0|,t), \quad (24)$$

where the Gaussian restricts x_0 and y_0 to a few σ_0, but does not limit the range of z_0 anymore.

We only need to consider long times $t \gg t_2 = \tau_c\sigma_0^3/l^3$. Then the initial wave packet is much narrower than the kernel, and for all values z_0 not much larger than σ_0, we find that the integral (22) is dominated by the contribution from the pole $\omega^{-1/3}$,

$$\int \frac{d\omega}{2\pi} \frac{\exp\{-i\omega t\}}{(-i\omega\tau_c)^{1/3}} = \frac{1}{\Gamma(1/3)(t^2\tau_c)^{1/3}}, \quad (25)$$

with the well-known $t^{-2/3}$ behavior [57,58,60]. What about large excursions in $z_0 \gg \sigma_0$? These are cut off by the anomalous propagator (22), via a saddle point of the integral, $P_c(z_0 \gg \sigma_0,t) \sim \exp\{-a(\sigma_0^3 t_2/z_0^3 t)^{1/2}\}$ (with a of order unity). The

resulting large-z_0 cutoff at $\sigma_0(t/t_2)^{1/3}$ of the remaining integral

$$\int_{\sigma_0}^{\sigma_0(t/t_2)^{1/3}} \frac{dz_0}{z_0} = \frac{1}{3}\ln(t/t_2), \quad (26)$$

then provides a logarithmic correction, which leads to

$$n_c^\perp(t) \sim n_0^\perp \Delta(t_2)\left(\frac{t_2}{t}\right)^{\frac{1+2\nu}{3\nu}} \ln\frac{t}{t_2}. \quad (27)$$

This result differs from the analogous estimate for the wings of density distributions [22], where the anomalous contribution is predicted to decay for $t \gg t_2$ as the pure power law $t^{-(1+2\nu)/3\nu}$, i.e., algebraically more slowly than the critical contribution, which disappears as $t^{-(1+3\nu)/3\nu}$. In the present setting of the central column density, with its additional integral over z, the signature of anomalous dynamics is only the logarithmic correction (27) to the critical power-law decay (19) with exponent $(1 + 2\nu)/3\nu \approx 0.875$.

IV. SUMMARY, OUTLOOK

In summary, we have discussed the specific challenges, and particular interest, of critical dynamics close to the 3D Anderson mobility edge in the expansion of noninteracting matter waves in strongly disordered laser speckle potentials. Given a certain spatial resolution σ_0, the critical Thouless time $t_1 = \sigma_0^2/D_c$ separates fast diffusion from a critical slowdown for dynamical observables. In particular, we find a crossover from a t^{-1} decay of the central column density to a $t^{-1/\nu}$ decay. The signature of anomalous dynamics emerges after the watershed time $t_2 = t_1\sigma_0/l_c$, where all localized components on scales smaller than σ_0 are frozen and all faster diffusive components have left, as a logarithmic correction on top of an accelerated critical background decaying as $t^{-(1+2\nu)/3\nu}$.

In our discussion, we have disregarded how exactly the localized components with $\xi_E < \sigma_0$ contribute to the transient dynamics of the central column density at times $t \ll t_2$, since the diffusive components are expected to dominate. However, it is certainly interesting to study the dynamics of atoms that will eventually localize in the wake of a quantum quench. From momentum-space coherence signatures of Anderson localization in lower dimensions $d \leqslant 2$ [61–65], we already know that the Heisenberg time of the localization volume appears as a relevant time scale. An exhaustive description of critical localization dynamics close to the 3D mobility edge is an interesting challenge for future theoretical work.

Also, we have neglected the possible impact of residual interactions. On a mean-field level, one expects that the localized fraction is replaced by a subdiffusive fraction, as discussed by Cherroret et al. in Ref. [66], including the possibility of different critical exponents. However, quantitative conclusions for the real-space measurement scenarios discussed presently have not yet been drawn, to our knowledge, and thus remain to be investigated.

ACKNOWLEDGMENTS

[1] P. W. Anderson, Phys. Rev. **109**, 1492 (1958).

[2] *50 Years of Anderson Localization*, edited by E. Abrahams (World Scientific, Singapore, 2010).

[3] E. Abrahams, P. W. Anderson, D. C. Licciardello, and T. V. Ramakrishnan, Phys. Rev. Lett. **42**, 673 (1979).

[4] F. Evers and A. D. Mirlin, Rev. Mod. Phys. **80**, 1355 (2008).

[5] P. A. Lee and T. V. Ramakrishnan, Rev. Mod. Phys. **57**, 287 (1985).

[6] D. Belitz and T. R. Kirkpatrick, Rev. Mod. Phys. **66**, 261 (1994).

[7] H. Hu, A. Strybulevych, J. H. Page, S. E. Skipetrov, and B. A. van Tiggelen, Nat. Phys. **4**, 945 (2008).

[8] D. S. Wiersma, P. Bartolini, A. Lagendijk, and R. Righini, Nature **390**, 671 (1997).

[9] M. Störzer, P. Gross, C. M. Aegerter, and G. Maret, Phys. Rev. Lett. **96**, 063904 (2006).

[10] T. Sperling, L. Schertel, M. Ackermann, G. J. Aubry, C. M. Aegerter, and G. Maret, New J. Phys. **18**, 013039 (2016).

[11] G. Modugno, Rep. Progr. Phys. **73**, 102401 (2010).

[12] B. Shapiro, J. Phys. A: Math. Theor. **45**, 143001 (2012).

[13] C. A. Müller and D. Delande, in *Ultracold Gases and Quantum Information: Lecture Notes of the Les Houches Summer School in Singapore:* Volume 91, edited by C. Miniatura, L.-C. Kwek, M. Ducloy, B. Grémaud, B.-G. Englert, L. Cugliandolo, A. Ekert, and K. K. Phua (Oxford University, Oxford, 2011), pp. 441–533.

[14] J. Chabé, G. Lemarié, B. Grémaud, D. Delande, P. Szriftgiser, and J. C. Garreau, Phys. Rev. Lett. **101**, 255702 (2008).

[15] G. Lemarié, B. Grémaud, and D. Delande, Europhys. Lett. **87**, 37007 (2009).

[16] S. S. Kondov, W. R. McGehee, J. J. Zirbel, and B. DeMarco, Science **334**, 66 (2011).

[17] F. Jendrzejewski, A. Bernard, K. Müller, P. Cheinet, V. Josse, M. Piraud, L. Pezzé, L. Sanchez-Palencia, A. Aspect, and P. Bouyer, Nat. Phys. **8**, 398 (2012).

[18] G. Semeghini, M. Landini, P. Castilho, S. Roy, G. Spagnolli, A. Trenkwalder, M. Fattori, M. Inguscio, and G. Modugno, Nat. Phys. **11**, 554 (2015).

[19] M. Piraud, P. Lugan, P. Bouyer, A. Aspect, and L. Sanchez-Palencia, Phys. Rev. A **83**, 031603 (2011).

[20] E. Akkermans and G. Montambaux, *Mesoscopic Physics of Electrons and Photons* (Cambridge University, Cambridge, England, 2007).

[21] R. Kuhn, O. Sigwarth, C. Miniatura, D. Delande, and C. A. Müller, New J. Phys. **9**, 161 (2007).

[22] S. E. Skipetrov, A. Minguzzi, B. A. van Tiggelen, and B. Shapiro, Phys. Rev. Lett. **100**, 165301 (2008).

[23] W. R. McGehee, S. S. Kondov, W. Xu, J. J. Zirbel, and B. DeMarco, Phys. Rev. Lett. **111**, 145303 (2013).

[24] C. A. Müller and B. Shapiro, Phys. Rev. Lett. **113**, 099601 (2014).

[25] W. R. McGehee, S. S. Kondov, W. Xu, J. J. Zirbel, and B. DeMarco, Phys. Rev. Lett. **113**, 099602 (2014).

[26] D. Delande and G. Orso, Phys. Rev. Lett. **113**, 060601 (2014).

[27] D. Basko, I. Aleiner, and B. Altshuler, Ann. Phys. (NY) **321**, 1126 (2006).

[28] R. Nandkishore and D. A. Huse, Annu. Rev. Cond. Mat. Phys. **6**, 15 (2015).

[29] E. Altman and R. Vosk, Annu. Rev. Cond. Mat. Phys. **6**, 383 (2015).

[30] M. Schreiber, S. S. Hodgman, P. Bordia, H. P. Lüschen, M. H. Fischer, R. Vosk, E. Altman, U. Schneider, and I. Bloch, Science **349**, 842 (2015).

[31] P. Bordia, H. P. Lüschen, S. S. Hodgman, M. Schreiber, I. Bloch, and U. Schneider, Phys. Rev. Lett. **116**, 140401 (2016).

[32] K. Agarwal, S. Gopalakrishnan, M. Knap, M. Müller, and E. Demler, Phys. Rev. Lett. **114**, 160401 (2015).

[33] A. C. Potter, R. Vasseur, and S. A. Parameswaran, Phys. Rev. X **5**, 031033 (2015).

[34] R. Vosk, D. A. Huse, and E. Altman, Phys. Rev. X **5**, 031032 (2015).

[35] Y. Bar Lev and D. R. Reichman, Europhys. Lett. **113**, 46001 (2016).

[36] J.-y. Choi, S. Hild, J. Zeiher, P. Schauß, A. Rubio-Abadal, T. Yefsah, V. Khemani, D. A. Huse, I. Bloch, and C. Gross, Science **352**, 1547 (2016).

[37] D. J. Luitz, N. Laflorencie, and F. Alet, Phys. Rev. B **93**, 060201 (2016).

[38] M. Piraud, L. Pezzé, and L. Sanchez-Palencia, Europhys. Lett. **99**, 50003 (2012).

[39] M. Piraud, L. Pezzé, and L. Sanchez-Palencia, New J. Phys. **15**, 075007 (2013).

[40] M. Piraud, L. Sanchez-Palencia, and B. van Tiggelen, Phys. Rev. A **90**, 063639 (2014).

[41] Strictly speaking, 3D speckle potentials created by a superposition of monochromatic beams from ideal rectangular or circular apertures, for which a white-noise limit does not exist, are not generic in this sense [21,12]. This caveat only affects the estimate (4) for the critical scale W, see [44], but does not invalidate our general analysis.

[42] A. Yedjour and B. A. Tiggelen, Eur. Phys. J. D **59**, 249 (2010).

[43] A simple on-shell approximation for the spectral function puts E_c above sea level [21], but this value is red-shifted below sea level by the real part of the single-particle self-energy [39].

[44] The estimate (4) holds for generic disorder. In nongeneric 3D speckle with an infrared divergence of the 3D pair correlator $C(\mathbf{k})$ [21], one rather has an energy-dependent mean free path $l_E \sim k_E \zeta^2/\eta^2$, such that $W \sim \eta^2 E_\xi = \eta V_0$, even larger than Eq. (4).

[45] M. I. Trappe, D. Delande, and C. A. Müller, J. Phys. A: Math. Theor. **48**, 245102 (2015).

[46] I. M. Lifshitz, Adv. Phys. **13**, 483 (1964).

[47] I. M. Lifshitz, S. A. Gredeskul, and L. A. Pastur, *Introduction to the Theory of Disordered Systems* (Wiley, New York, 1988).

[48] M. Pasek, Z. Zhao, D. Delande, and G. Orso, Phys. Rev. A **92**, 053618 (2015).

[49] K. Slevin and T. Ohtsuki, Phys. Rev. Lett. **82**, 382 (1999).

[50] A. Rodriguez, L. J. Vasquez, K. Slevin, and R. A. Römer, Phys. Rev. Lett. **105**, 046403 (2010).

[51] M. Lopez, J.-F. Clément, P. Szriftgiser, J. C. Garreau, and D. Delande, Phys. Rev. Lett. **108**, 095701 (2012).

[52] K. Slevin and T. Ohtsuki, New J. Phys. **16**, 015012 (2014).

[53] F. J. Wegner, Z. Phys. B **25**, 327 (1976).

[54] B. Kramer and A. MacKinnon, Rep. Progr. Phys. **56**, 1469 (1993).

[55] C. Soukoulis and E. Economou, Waves Rand. Media **9**, 255 (1999).

[56] K. Efetov, *Supersymmetry in Disorder and Chaos* (Cambridge University, Cambridge, England, 1997).

[57] T. Ohtsuki and T. Kawarabayashi, J. Phys. Soc. Jpn. **66**, 314 (1997).

[58] G. Lemarié, H. Lignier, D. Delande, P. Szriftgiser, and J. C. Garreau, Phys. Rev. Lett. **105**, 090601 (2010).

[59] B. Shapiro, Phys. Rev. B **25**, 4266 (1982).

[60] G. Lemarié, J. Chabé, P. Szriftgiser, J. C. Garreau, B. Grémaud, and D. Delande, Phys. Rev. A **80**, 043626 (2009).

[61] T. Karpiuk, N. Cherroret, K. L. Lee, B. Grémaud, C. A. Müller, and C. Miniatura, Phys. Rev. Lett. **109**, 190601 (2012).

[62] K. L. Lee, B. Grémaud, and C. Miniatura, Phys. Rev. A **90**, 043605 (2014).

[63] S. Ghosh, N. Cherroret, B. Grémaud, C. Miniatura, and D. Delande, Phys. Rev. A **90**, 063602 (2014).

[64] T. Micklitz, C. A. Müller, and A. Altland, Phys. Rev. Lett. **112**, 110602 (2014).

[65] T. Micklitz, C. A. Müller, and A. Altland, Phys. Rev. B **91**, 064203 (2015).

[66] N. Cherroret, B. Vermersch, J. C. Garreau, and D. Delande, Phys. Rev. Lett. **112**, 170603 (2014).